RSC Advances

PAPER

View Article Online
View Journal | View Issue

Cite this: *RSC Adv.*, 2022, **12**, 16544

A facile route to synthesize n-SnO_2/p-$CuFe_2O_4$ to rapidly degrade toxic methylene blue dye under natural sunlight†

Kaijiao Duan,[a] Tingting Que,[a] Sivasankar Koppala, *[b] Ramdas Balan,*[c] Budigi Lokesh,[d] Rahul Pillai,[ef] Selvaraj David,[g] Parasuraman Karthikeyan, [h] Sangeetha Ramamoorthy,[ef] I. C. Lekshmi,[e] Patiya Kemacheevakul,[i] Nagarajan Padmavathy[j] and Sathishkumar Munusamy[k]

In the present study, the n-SnO_2/p-$CuFe_2O_4$ (p-CFO) complex was prepared by a two-step process. p-CFO synthesized by the molten salt method was coated with SnO_2 synthesized by a facile *in situ* chemical precipitation method. The formation of n-SnO_2/p-CFO was confirmed by powder X-ray diffraction (PXRD). Scanning electron microscopy (SEM) images showed that the sharp edges of uncoated pyramid-like p-CFO particles were covered by a thick layer of n-SnO_2 on coated p-CFO particles. The complete absence of Cu and only 3 wt% Fe on the surface of the n–p complex observed in the elemental analysis using energy-dispersive X-ray spectroscopy (EDX) on the n–p complex confirmed the presence of a thick layer of SnO_2 on the p-CFO surface. Diffuse reflectance spectroscopy (DRS) was employed to elucidate the bandgap engineering. The n-SnO_2/p-CFO complex and p-CFO showed 87% and 58.7% methylene blue (MB) degradation in 120 min under sunlight, respectively. The efficiency of the n–p complex recovered after 5 cycles (73.5%) and was found to be higher than that of the uncoated p-CFO (58.7%). The magnetically separable property of the n–p complex was evaluated by using vibration sample magnetometry (VSM) measurements and it was confirmed that the prepared photocatalyst can be easily recovered using an external magnet. The study reveals that the prepared complex could be a potential candidate for efficient photodegradation of organic dyes under sunlight due to its efficient recovery and reusability owing to its magnetic properties.

Received 18th March 2022
Accepted 11th May 2022

DOI: 10.1039/d2ra01690g

rsc.li/rsc-advances

1 Introduction

The development of catalysts for the effective degradation of organic dye pollutants in wastewater is one of the promising research topics in the arena of environmental remediation. Among various organic dyes, methylene blue is a phenothiazine derivative that is highly toxic, carcinogenic, and predominant in industrial effluents which could cause serious health hazards upon intake.[1] Traditional techniques such as ozonation, adsorption, *etc.* cannot eliminate the toxicity of these dyes due to various constraints.[2] The development of photocatalysts for degradation of these dyes is one of the methods recently developed which uses direct solar energy as a source for effective degradation.[3] Amidst different classes of materials, metal oxides such as TiO_2 and ZnO are well-known semiconductor photocatalysts for dye degradation.[3–8] Tin oxide (SnO_2) is an n-type metal oxide well-studied photocatalyst for dye degradation owing to its superior optical, electrical, and electrochemical properties.[9–13] It is a viable photocatalyst for practical applications due to facile production, low cost, eco-friendly, good chemical and biological inertness, high photosensitivity, and thermodynamic stability.[14,15] Nevertheless, separating the

[a]*School of Chemistry and Environment, Yunnan Minzu University, Kunming 650505, Yunnan, China*
[b]*Saveetha School of Engineering, Saveetha Institute of Medical and Technical Sciences (SIMATS), Chennai 602105, Tamil Nadu, India. E-mail: pepsiva9@gmail.com*
[c]*Department of Physics, CMR Institute of Technology, Bengaluru 560037, Karnataka, India. E-mail: balan.ramdas@gmail.com*
[d]*Department of Chemistry, MVJ College of Engineering, Bengaluru 560067, Karnataka, India*
[e]*CoE Materials Science/Sensors & Nanoelectronics, Department of Chemistry, CMR Institute of Technology, Bengaluru 560037, Karnataka, India*
[f]*VTU-Research Centre Affiliated to Visvesvaraya Technological University, Belagavi 590018, Karnataka, India*
[g]*Department of Chemistry, Periyar University, Salem 636011, Tamilnadu, India*
[h]*PG and Research Department of Chemistry, Pachaiyappas College, University of Madras, Chennai 600030, Tamilnadu, India*
[i]*Department of Environmental Engineering, Faculty of Engineering, King Mongkut's University of Technology Thonburi, Bangkok 10140, Thailand*
[j]*Department of Materials Engineering, Indian Institute of Science, Bengaluru 560012, India*
[k]*Department of Chemistry, Faculty of Science, Chulalongkorn University, Pathumwan, Bangkok, 10330, Thailand*

† Electronic supplementary information (ESI) available. See https://doi.org/10.1039/d2ra01690g

photocatalyst from treated water and reuse is challenging, especially in the nano-form due to its high dispersive nature. In these cases, magnetic photocatalysts are advantageous owing to their ease of separation post usage. Therefore, magnetic spinel ferrites such as MFe_2O_4 (M = Cu, Co, Zn, Mn, Ni) have gained considerable attention.[16–18] $CuFe_2O_4$ (CFO) is one of the important inverse spinel ferrite a p-type material possessing attractive magnetic, electronic, and optical properties; studied as a catalyst for a variety of applications including reduction,[19] oxidation,[20] photocatalytic hydrogen production,[21] and photocatalytic degradation of dyes.[22–25] Unfortunately, CFO has a low quantum efficiency due to the rapid recombination of photogenerated electron–hole pairs. This separation of the electron–hole pairs can be improved by transition metal graft or composite to form heterojunction or complex formation.[26–33] Mostly, p–n type heterojunction of composites materials were reported to have effective photogenerated electrons/holes separation due to electric field created in the junction *in virtue* to enhance the photocatalytic activity.[34–36] Few example for the p-type CFO utilized to decorated the diverse metal oxides and applicable to the various research field in recent universe; TiO_2/CFO,[37,38] RGO/CFO/TiO_2,[39] ZnO/CFO,[40] CFO/PAMAM (polyaminodoamine dendrimers),[41] $CuFe_2O_4$/$Bi_4Ti_3O_{12}$.[27,31,42] Limited work was reported for n-SnO_2/p-CFO; it was used for sensing, optical, and enhancing the electrical properties of the sample.[43–45] Up to the author's knowledge, there was no coherent application reported for the past decade. We have constructed the n–p type complex instead of the p–n type and used it for the environmental remediation of toxic dyes.

In the present work, the n-SnO_2/p-CFO complex was successfully synthesized by a two-step process, first p-CFO microcrystals were prepared by the molten salt method, and secondly, *in situ* n-SnO_2 was grown on p-CFO by chemical precipitation method. The photocatalytic activity was investigated for the prepared n-SnO_2/p-CFO complex under natural sunlight for photodegradation of methylene blue (MB) dye. n-SnO_2/p-CFO complex showed higher catalytic activity under direct sunlight than p-CFO due to the formation of the n–p complex. The magnetic property of the composite enables the easy recovery of the composite from the water body for reuse. To the best of our knowledge, there is no prior reported literature on the facile preparation of n-SnO_2/p-CFO photocatalyst and its application in MB dye degradation under natural sunlight irradiation. The proposed charge separation mechanism was declared the photocatalytic degradation of organic dyes.

2 Experiment work

Analytical reagent (AR) graded chemicals were employed to develop the complex formation with the below experiments. The prepared compounds were characterized using techniques such as powder X-ray diffraction (PXRD, Bruker D2 phaser, at scan speed 0.5° min^{-1}), scanning electron microscopy (SEM, ZEISS Ultra-55), diffuse reflectance spectrometry (DRS, PerkinElmer, lambda 365 spectrophotometer), Electrochemical workstation (CHI660E, CH Instruments), vibrating sample magnetometer (VSM, Lakeshore) at room temperature (27 °C, RT) for applied magnetic field ranges from −0.5 Tesla to +0.5 Tesla.

2.1 Preparation of p-CFO

The p-type $CuFe_2O_4$ (p-CFO) was prepared by the molten salt synthesis (MSS) method using Cu_2O (Thomas Baker, India), Fe_2O_3 (Thomas Baker, India), NaCl (Thomas Baker, India), and KCl (Thomas Baker, India) chemicals. The stoichiometric ratio of 1 : 2 starting materials *i.e.*, 1.430 g of Cu_2O and 3.139 g of Fe_2O_3 were ground in the agate pestle mortar in the ethanol medium for 1 hour. The dried mixture powder was put along with the eutectic mixture of the mediator, 5.727 g of NaCl and 7.604 g of KCl in a 100 ml capacity recrystallized alumina crucible and heat-treated at 900 °C for 6 h inside the muffle furnace and allowed furnace cool. The solidified molten salt was dissolved and washed with a copious quantity of deionized water to remove mediator alkali chloride salts. The residue black mass was dried in a hot air oven overnight.

2.2 Preparation of n-SnO_2/p-$CuFe_2O_4$ complex

First, the Sodium stannate solution was prepared by dissolving 5 g of $Na_2SnO_3 \cdot 2H_2O$ (SD fine chemicals) in 100 ml of distilled water and adding 5 ml of hydrazine hydrate (SD fine chemicals). Followed by 1 g of p-CFO microcrystals were added to the transparent sodium stannate solution and stirred for 1 h. The p-CFO mixed solution was kept undisturbed for the growth of n-SnO_2 on p-CFO microcrystals, assisted with intermediate ultrasonication. The resultant white slurry was washed with copious distilled water, and later magnetically separated and dried at 80 °C overnight in an oven. Post drying, the sample was heat-treated at 500 °C for 6 h resulting in fine powder which was later used for further characterization and photocatalytic studies. The proposed schematic diagram was illustrated in Fig. 1.

2.3 Photocatalytic studies

The photocatalytic performance of the prepared catalysts was evaluated for MB dye degradation under sunlight exposure. In the present study, 100 mg of the prepared photocatalyst was suspended in 100 ml of 3 mg L^{-1} MB dye solution. The suspension was agitated at 200 rpm using a magnetic stirrer (REMI 5 ML) in dark conditions for 30 minutes to achieve dye adsorption–desorption equilibrium on the composite photocatalyst.[46,47] Post adsorption–desorption equilibria, the suspension was positioned in an open place under direct sunlight between 11 a.m. to 1 p.m. as per Indian Standard Time (IST). During this process, periodically 5 ml of suspension were extracted and the solution was recorded using a UV-Vis spectrophotometer to quantify the MB dye content by measuring absorbance at 663 nm. The used photocatalyst was recovered from the treated MB solution with the aid of a magnet (magnetic strength = 0.3 Tesla), washed with distilled water, and dried at 100 °C overnight. The photocatalytic experiments were repeated in the same conditions using a recovered catalyst to check the reusability. Scavenger test was performed maintaining same photocatalytic experiment condition with the

Fig. 1 Schematic diagram represents the facile route to prepare the n-SnO_2/p-CFO complex.

addition of scavengers such as benzoquinone (BQ), potassium iodine (KI), potassium bromate ($KBrO_3$), and isopropanol (IPA) for effective charge separation (e^-/h^+) provide enormous radicals; such as superoxide and hydroxyl radical respectively.

The efficiency of the dye degradation was calculated using the expression

$$\%\ \text{degradation} = (C_0 - C_t)/C_0 \times 100 \quad (1)$$

where C_0 is the initial absorbance, and C_t is the absorbance at time t.

3 Results and discussion

3.1 Characterization

3.1.1 XRD studies. The XRD pattern of the core compound prepared by MSS using a eutectic mixture of NaCl–KCl mediated salts is depicted in Fig. 2b. The pattern is consistent with the standard data of p-CFO (Fig. 2c), confirming the formation of the pure cubic-p-CFO phase. The diffraction pattern of the n-SnO_2/p-CFO complex is shown in Fig. 2a. The diffraction peaks detected at 26.64°, 33.88°,51.8°, 57.82°, 64.92°, and 66.02° are consistent with n-SnO_2 of tetragonal structure P42mnm space group (136); the standard SnO_2 data shown in Fig. 1d.[48] The other four peaks observed at 35.52°, 42.13°, 57.1°, and 62.74° attribute to cubic-p-CFO diffraction planes (311), (400), (511), and (440), respectively.[49] The peak intensity of the p-CFO is relatively weak due to the *in situ* deposition of n-SnO_2 on the p-CFO. The peak profile of n-SnO_2 was observed to be broadened, which affirms that it is in nano-crystalline form.

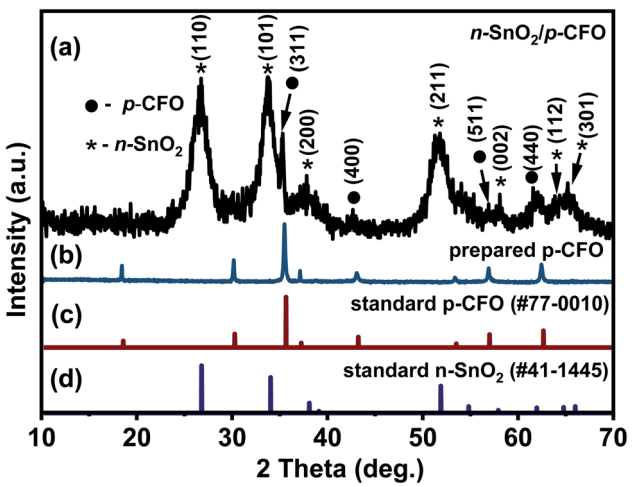

Fig. 2 Shows the XRD pattern of (a) prepared n-SnO_2/p-CFO complex, (b) prepared p-CFO, (c) standard p-CFO pattern, and (d) standard n-SnO_2 pattern.

3.1.2 Scanning electron microscope studies. Fig. 3 shows the SEM images of the p-CFO and p-CFO coated with n-SnO_2. Uncoated p-CFO particles are micron size pyramidal shape particles with sharp edges as shown in Fig. 3a. p-CFO particles coated with n-SnO_2 revealed smooth surfaces indicating that the sharp edges of p-CFO are covered by a thick layer of n-SnO_2 as shown in Fig. 3b. From the EDX pattern of n-SnO_2/p-CFO shown in the ESI (Fig. S1†) it is observed that only 3 wt% of Fe was observed and Cu was completely absent, confirming the formation of a thick layer of n-SnO_2 on p-CFO surface resulting in n–p complex.[44]

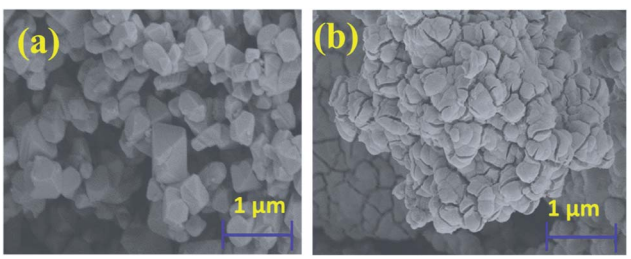

Fig. 3 SEM image of (a) p-CFO and (b) n-SnO_2/p-CFO complex.

3.1.3 Calculation of optical band gap. The Kubelka–Munk (K–M function, eqn (2))[50,51] was used to find the bandgap of the prepared p-CFO and n-SnO_2/p-CFO complex.

$$(\alpha h\nu)^n = A(h\nu - E_g) \quad (2)$$

where n is determined from the type of optical transition of a semiconductor ($n = 2$ for direct transition and $n = 1/2$ for indirect transition), while α, $h\nu$ and E_g are the absorption coefficient, the incident photon energy, and the bandgap energy, respectively; A is a constant. Fig. 4a and b show the K–M plot, *i.e.*, $(\alpha h\nu)^2$ plotted against the photon energy ($h\nu$) of p-CFO and n-SnO_2/p-CFO complex respectively. From the plots, the energy bandgap was derived by taking tangent from the linear part of the curve intercepting the x-axis and the values found were 1.83 eV and 3.22 eV for p-CFO and n-SnO_2/p-CFO respectively. The optical bandgap of the n-SnO_2/p-CFO complex is more than p-CFO and less than that of the bulk n-SnO_2 (3.6 eV) attributing to the formation of complex structure. The optimum encapsulation of the bare sample can reduce the bandgap of the pristine materials.[52,53] However, the bandgap is closer to the bulk n-SnO_2, due to the dominant shell formation of SnO_2 which is in agreement with XRD & SEM analysis. Additionally, the clear scheme for the band position and charge separation mechanism was designated in Fig. 7.

3.1.4 Magnetic studies. Fig. 5 depicts the hysteresis curves of the prepared p-CFO and n-SnO_2/p-CFO complex. The VSM measurement was carried out at room temperature for magnetic field range from −0.5 to +0.5 Tesla. The saturation magnetization (Ms) values for p-CFO and n-SnO_2/p-CFO were determined to be 17.44 emu g^{-1} and 8.9965 emu g^{-1}, respectively. M_s value generally implies the ease with which powder can be recovered with an external magnetic field. The coercivity (H_c) and retentivity (M_R) of the n-SnO_2/p-CFO composite are 0.017 Tesla and 2.90 emu g^{-1} respectively. These values are diminution compared to p-CFO, which is 0.038 Tesla and M_R = 6.13 emu g^{-1}. This is due to the presence of the nonmagnetic compound SnO_2 in the complex. However, the magnetic characteristics of the resulting complex are sufficient to separate the composite magnetically post photocatalytic process which is highly recommended for recovery and reusability for sustainable utility (illustrated in inset Fig. 5).

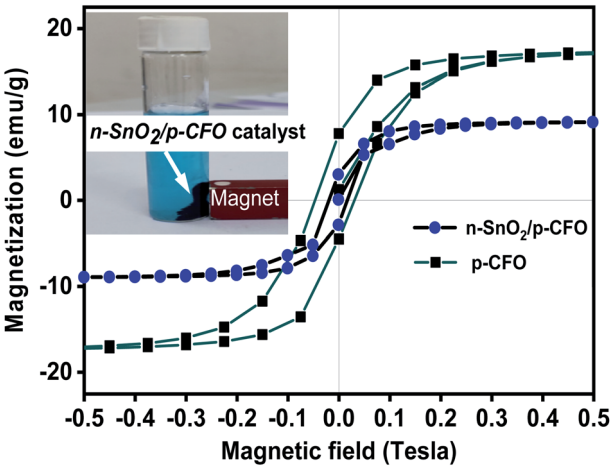

Fig. 5 Hysteresis curves of the prepared p-CFO and n-SnO_2/p-CFO complex.

3.2 Photocatalytic degradation evaluation

Fig. 6a and b shows the absorption spectrum of MB dye drawn during the photocatalysis under sunlight by p-CFO and n-SnO_2/p-CFO catalyst respectively. It is observed that the intensity of the absorption peak at 663 nm gradually decreased concerning catalytic time. The photocatalytic degradation efficiency plot (C_t/C_0 *vs.* time) of the studied catalysts is shown in Fig. 6c. The maximum MB degradation of the p-CFO and n-SnO_2/p-CFO photocatalysts were observed 58.7% and 87% respectively at 120 min which revealed superior photocatalytic activity of n-SnO_2/p-CFO photocatalyst. Photodegradation of MB dye without the presence of catalyst conducted in the sunlight showed less than 5% degradation of the dye, which indicates the efficiency of the prepared photocatalyst.

The photodegradation of dyes usually follows pseudo-first-order kinetics and we analyzed this behavior for our reaction studies.

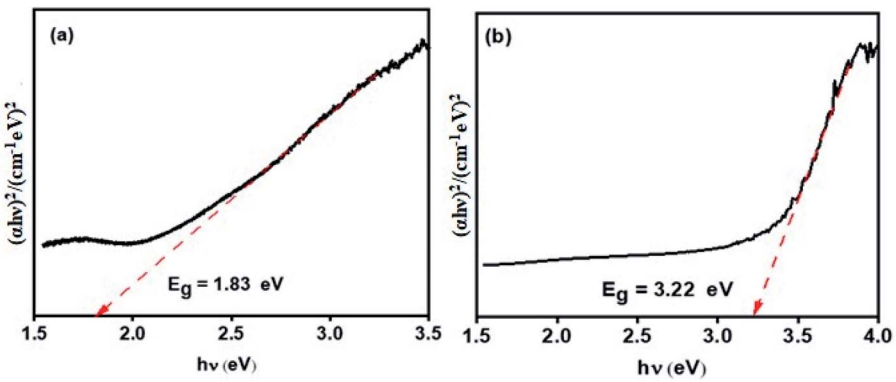

Fig. 4 Kubelka–Munk plot for (a) p-CFO (narrow band gap) and, (b) n-SnO_2/p-CFO (wide band gap).

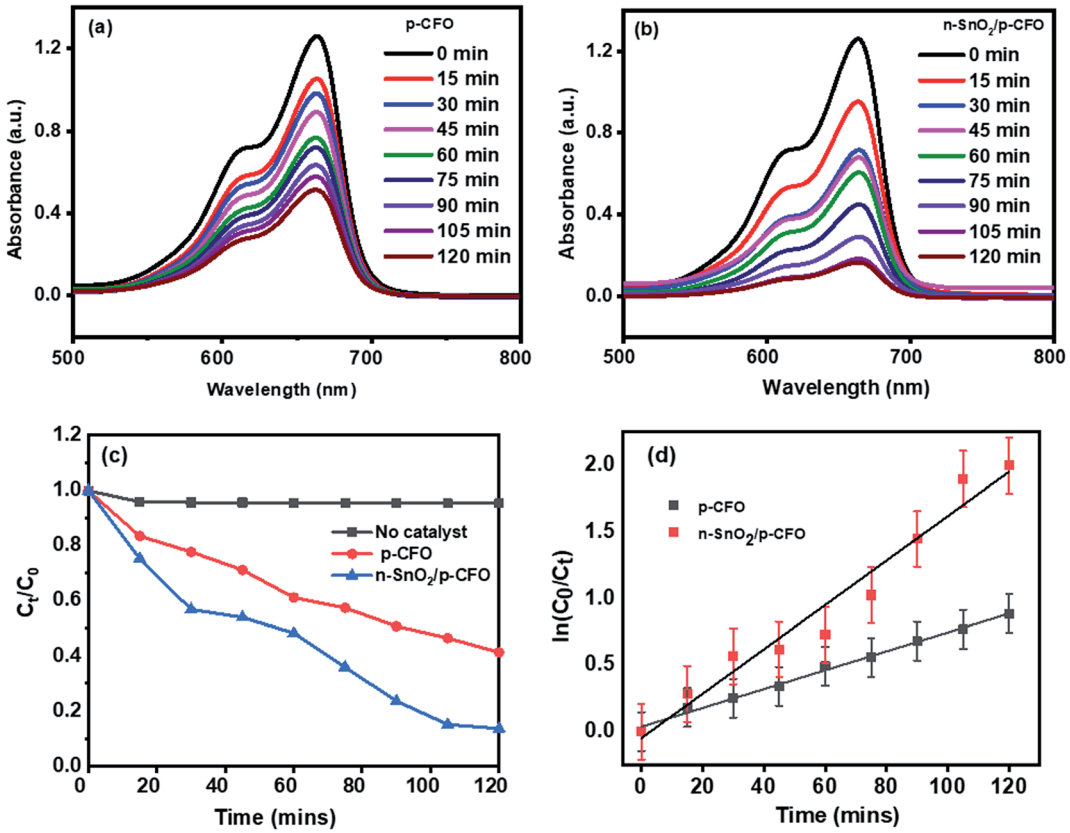

Fig. 6 Photocatalytic MB dye degradation under direct sunlight irradiation (a) p-CFO, (b) n-SnO_2/p-CFO, (c) C_t/C_0 plot, (d) ln C_0/C_t *vs.* time plot for the determination of rate constant.

$$R = -\frac{dC}{dt} = k_0 C \quad (3)$$

$$-\ln\frac{C_t}{C_0} = k_0 t \quad (4)$$

where C_0 and C_t denoted the initial dye solution concentration and concentration at the time respectively. The plot of $\ln(C_0/C_t)$ *versus* time for all photocatalysis with 3 ppm dye concentration and 100 mg/100 ml catalyst concentration was observed as a linear plot with a correlation coefficient (R^2) of 0.95–0.99 confirming their pseudo-first-order kinetics. The n-SnO_2/p-CFO complex showed the steepest slope for the photodegradation kinetics as shown in Fig. 6d implying the high catalytic ability. The relevant parameters of photodegradation kinetics for different photocatalysts are shown in Table 1. The photocatalytic activities of TiO_2, ZnO, MFe_2O_4 (M = Mn, Cu, Ni, Co, Zn) were presented in a Table 2 for comparison.

Table 1 Kinetic rate constant for p-CFO and n-SnO_2/p-CFO complex

Compound prepared	Rate constant (K min^{-1})	Correlation coefficient (R^2)
CFO	0.00708	0.9937
n-SnO_2/p-CFO	0.01665	0.9615

3.2.1 Reusability and scavengers studies of the photocatalyst. The recovered n-SnO_2/p-CFO complex catalyst was studied for recyclability for two cycles and the results are depicted in Fig. 7a. The results represented consecutive cycles with 85.2%, 83.9%, 78.3% and 73.5% efficiency suggesting excellent reusability of the prepared catalyst. The XRD pattern of the used catalyst after 5 cycles is shown in ESI, Fig. S2,† it depicts decrement in the intensity of the surface coated SnO_2 peaks due to which the efficiency is droped to 73.5%. The scavenger test was carried out for n-SnO_2/p-CFO to identify the reactive species involved in this photocatalysis mechanism by the addition of scavengers such as benzoquinone (BQ), potassium iodide (KI), potassium bromate ($KBrO_3$), and isopropanol IPA for $^{\bullet}O_2$, h^+, e^- and $^{\bullet}OH$ respectively. The scavenger test plot of MB degradation percentage was calculated with and without scavengers for n-SnO_2/p-CFO complex is shown in Fig. 7b. The degradation efficiencies were greatly prevented by KI (77.5%), and a meager decrease by the addition of $KBrO_3$ (3.5%), IPA (1.5%), and BQ (15.3%). Thus, these result of the trapping experiments under the sunlight demonstrates the photogenerated holes (h^+) are the main active species triggering the photocatalytic degradation reaction to take place on the surface of the photocatalyst.

Table 2 Comparison of photocatalytic/catalytic activity of ZnO, TiO_2, SnO_2, and MFe_2O_4[a]

S. No	Material	Dye	Degradation (%)	Irradiation source	Time (min)	Reference
1	ZnO	MB	93			8
2	TiO_2	MB	66	UV ($\lambda = 254$ nm)	180	3
3	ZnO	MB, MO	Degradation rate is proportional to UV intensity	UV ($\lambda = 365$ nm)		5
4	Calcined abalone shell with 23.4% TiO_2 loading	MB	100	Natural sunlight	140	7
5	SnO_2	MB	100	UV ($\lambda = 365$ nm)	70	11
6	SnO_2	Congo red	90	UV ($\lambda = 365$ nm)		13
	TiO_2 degussa P-25		88			
7	SnO_2	MB	3.8 time better activity than bulk SnO_2	UV ($\lambda = 365$ nm)		12
8	SnO_2	RhB	92	UV ($\lambda = 365$ nm)	120	10
9	SnO_2	MB	98.5	Natural sunlight	80	51
10	SnO_2	RB	99.3	Natural sunlight	180	15
		MB	96.8		240	
11	$ZnFe_2O_4$	RhB	98	UV ($\lambda = 365$ nm)	120	15
12	$MnFe_2O_4$	Direct red 81 dye	56.5	Natural sunlight	120	16
13	$CuFe_2O_4$	Acidic orange	87.6	Catalyst for reduction of organic compounds		18
14	MFe_2O_4 spinel (M = Cu, Ni, Co, Zn)		100	Catalytic reduction of 4-nitrophenol		19
15	Core–shell carbon dot@MFe_2O_4 (M = Mn, Zn and Cu)		>95	Catalytic reduction of *p*-nitropheno		25
18	p-$CuFe_2O_4$	MB	58.7	Natural sunlight	120 min	This work
19	n-SnO_2/p-$CuFe_2O_4$	MB	87	Natural sunlight	120 min	This work

[a] MB: methylene blue; MO: methyl orange; RB: rose bengal; RhB: rhodamine B.

3.2.2 Plausible mechanism of photodegradation. Photocatalyst constitutes tetragonal-SnO_2 (n-type semiconductor) and cubic-$CuFe_2O_4$ (p-type semiconductor) semiconductors having band gap of 3.22 eV and 1.83 eV respectively. SEM micrograph and optical band gap of the SnO_2/CFO confirms that SnO_2 is completely coated on CFO. Hence, the thick SnO_2 coating forbids maximum light reaching the inner core c-CFO. Therefore, SnO_2/CFO suspension solution under sunlight promotes the formation of electrons in the conduction band (CB,e_{CB}^-) and holes in the valence band (VB,h_{VB}^+) of the SnO_2 (eqn (5)).

$$SnO_2 + h\nu \rightarrow e_{CB}^- + h_{VB}^+ \quad (5)$$

The potential values of EVB and ECB of the semiconductors dictates reduction and oxidation of the photogenerated electron – holes in the degradation process.[30,31] It was calculated using eqn (6) and (7).

$$ECB = \chi - E^e - 0.5E_g \quad (6)$$

$$EVB = ECB + E_g \quad (7)$$

where E_g is the optical band gap calculated from the K–M plot, E^e is the energy of free electrons on the NHE scale factor (*i.e.*, 4.50 eV), and χ is the absolute electronegativity of the semiconductor. The calculated values of the ECB and EVB for c-CFO are −1.42 eV and 0.41 eV, and for SnO_2 coated on the composite, the values are 0.14 eV and 3.36 eV. The band diagram is shown in the Fig. 6c. The potential ECB of the CFO in SnO_2/CFO is more negative than the reduction potential of $O_2/^{\bullet}O_2$ (−0.33 eV vs. NHE) and the EVB of SnO_2/CFO is more positive than the oxidation potential of $H_2O/^{\bullet}OH$ (+2.7 eV vs. NHE). Moreover, coupling of two different types of semiconductors forms a p–n junction and the photoexcited electrons from the CB of SnO_2 combines with the holes generated from CFO by the driving force due to the inner electric field and could be attributed to Z-scheme mechanism.[32] Hence, the photogenerated electrons in the higher CB edge of CFO and the higher VB edge of SnO_2 could take part in the reduction and oxidation reaction of the MB dye. In addition, scavenger test confirmed the role of holes as major reactive species which paved the evident path to Z-scheme mechanism. During the scavenger test post addition of KI scavenger for holes there was dramatic decrease in the % dye removal suggesting holes were the dominant active species, BQ had considerable effect and IPA had weak effect implying superoxide radicals and hydroxyl radicals are also vital to elucidate the Z-scheme mechanism. The flow of electrons was further confirmed by the interface formation of p–n junction using EIS spectroscopy by varying the frequency from 1–106 Hz with standard 3-electrode set-up. The Nyquist plot showed in ESI, Fig. S3† represents two semi circles. One with a lager diameter which corresponds to c-CFO and the other smaller one due to the SnO_2/CFO composite. The decrement in the semicircle in case of the composite indicates the fast flow of electrons compared to the parent material suggesting the formation

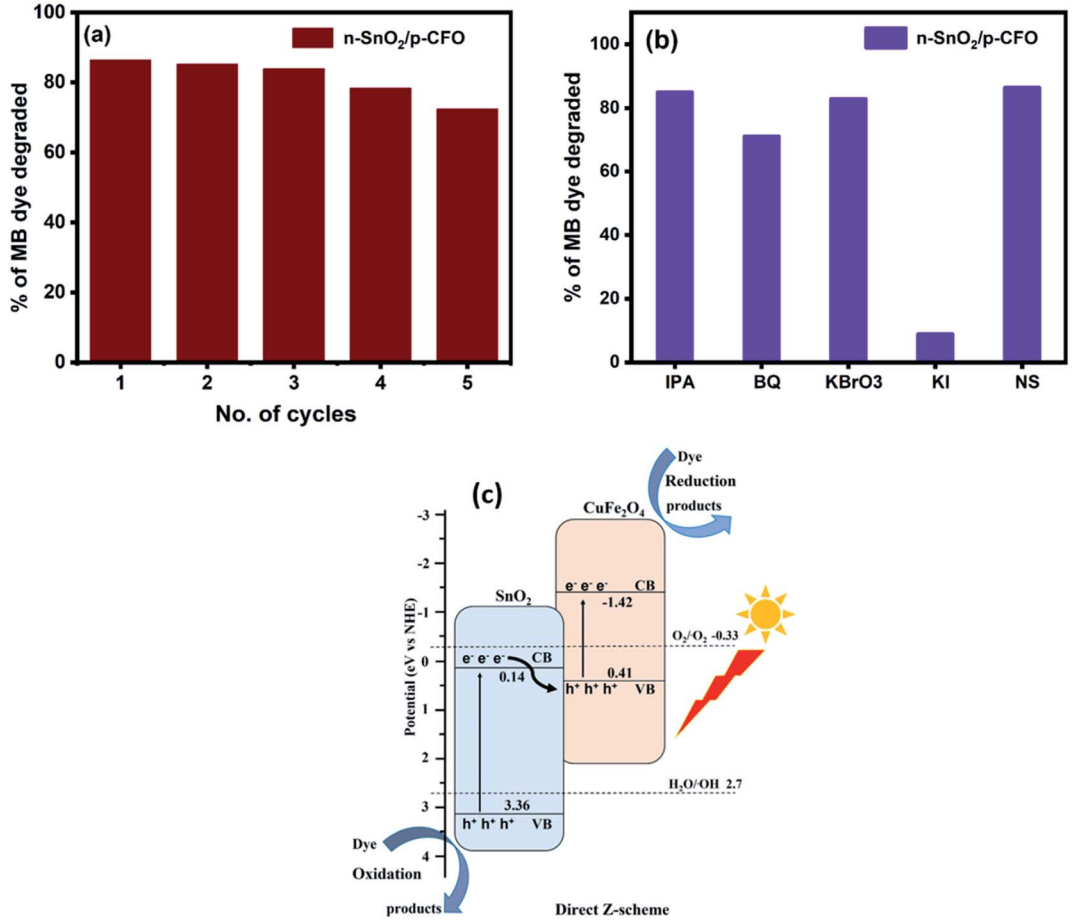

Fig. 7 Depicts the photocatalytic MB degradation for (a) reusability (b) degradation percentage for various samples and (c) indicates the energy band scheme for n-SnO_2/p-CFO complex.

of a localized p–n junction interface which is assisting the easy passage of photoelectrons generated on the surface of the shell SnO_2. The separated photogenerated holes in the valence band (h_{VB}^+) on the SnO_2 will oxidize MB dye molecules directly due to their strong oxidizing ability (eqn (8)).[33]

$$h_{VB}^+ + MB \rightarrow MB^{+\cdot} \quad (8)$$

The n–p complex got better charge transport; the reaction mechanism was elaborately discussed in the below box.

4 Conclusions

Photocatalyst n-SnO_2/p-CFO complex synthesized *via* a two-step process *i.e.*, molten salt synthesis of p-CFO followed by n-SnO_2 by chemical precipitation method was characterized by powder XRD, SEM, EDX, and DRS. MB dye degradation studies under sunlight confirmed that the n–p complex is a more efficient photocatalyst (87%) than the uncoated p-CFO (58.7%) with better recovery and reusability properties and follows pseudo first order kinetics. Decrease in efficiency of the recovered photocatalyst after 5 cycles (73.5%) is due to loss of SnO_2 from the surface of n–p complex as evidenced from the powder XRD patterns of the recovered n–p complex. This indicates that the n-SnO_2 plays a major role in photocatalytic activity and p-CFO helps in easy recovery of the photocatalyst by magnetic separation as evidenced in VSM measurements. The scavenger and EIS studies revealed the role of photogenerated holes in the complex structure forming a localized n–p junction at the interface by the synergetic effect of n-SnO_2 and p-CFO thereby preventing the recombination process. This study depicts the use of magnetically separable n–p complex n-SnO_2/p-CFO as a potential catalyst candidate for the photodegradation of organic dyes under sunlight.

Author contributions

Kaijiao Duan: methodology, investigation, reviewing and editing; Tingting Que: methodology, investigation, reviewing and editing; Sivasankar Koppala: conceptualization, methodology, investigation, project administration, writing – original draft preparation, supervision; Ramdas Balan: conceptualization, data curation, investigation, writing – original draft preparation, supervision; Budigi Lokesh: investigation, writing – original draft preparation; resources; Rahul Pillai: formal analysis, writing – reviewing; Selvaraj David: reviewing and editing;

Parasuraman Karthikeyan: reviewing and editing; S. Ramamoorthy: resources; I. C. Lekshmi: resources; Patiya Kemacheevakul: reviewing and editing; Nagarajan Padmavathy: resources; Sathishkumar Munusamy: reviewing and editing.

Conflicts of interest

There are no conflicts to declare.

Acknowledgements

Authors acknowledge the support of YMU, CMRIT and SIMATS.

References

1 B. Appavu, S. Thiripuranthagan, S. Ranganathan, E. Erusappan and K. Kannan, BiVO4/N-rGO nano composites as highly efficient visible active photocatalyst for the degradation of dyes and antibiotics in eco system, *Ecotoxicol. Environ. Saf.*, 2018, **151**, 118–126.

2 E. Brillas and C. A. Martínez-Huitle, Decontamination of wastewaters containing synthetic organic dyes by electrochemical methods. An updated review, *Appl. Catal. B Environ.*, 2015, **166**, 603–643.

3 C. P. M. de Oliveira, A. L. A. Lage, D. C. da Silva Martins, N. D. S. Mohallem and M. M. Viana, High surface area TiO2 nanoparticles: impact of carboxylporphyrin sensitizers in the photocatalytic activity, *Surface. Interfac.*, 2020, **21**, 100774.

4 J. Schneider, M. Matsuoka, M. Takeuchi, J. Zhang, Y. Horiuchi, M. Anpo, *et al.*, Understanding TiO2 photocatalysis: mechanisms and materials, *Chem. Rev.*, 2014, **114**(19), 9919–9986.

5 J. Kegel, V. Z. Zubialevich, M. Schmidt, I. M. Povey and M. E. Pemble, Effect of surface and defect chemistry on the photocatalytic properties of intentionally defect-rich ZnO nanorod arrays, *ACS Appl. Mater. Interfaces*, 2018, **10**(21), 17994–18004.

6 K. Ancy, M. R. Bindhu, J. S. Bai, M. K. Gatasheh, A. A. Hatamleh and S. Ilavenil, Photocatalytic degradation of organic synthetic dyes and textile dyeing waste water by Al and F co-doped TiO2 nanoparticles, *Environ. Res.*, 2022, **206**, 112492.

7 W. Wang, F. Lin, B. Yan, Z. Cheng, G. Chen, M. Kuang, *et al.*, The role of seashell wastes in TiO2/Seashell composites: Photocatalytic degradation of methylene blue dye under sunlight, *Environ. Res.*, 2020, **188**, 109831.

8 F. Ameen, T. Dawoud and S. AlNadhari, Ecofriendly and low-cost synthesis of ZnO nanoparticles from Acremonium potronii for the photocatalytic degradation of azo dyes, *Environ. Res.*, 2021, **202**, 111700.

9 V. Perumal, C. Inmozhi, R. Uthrakumar, R. Robert, M. Chandrasekar, S. B. Mohamed, *et al.*, Enhancing the photocatalytic performance of surface - Treated SnO2 hierarchical nanorods against methylene blue dye under solar irradiation and biological degradation, *Environ. Res.*, 2022, **209**, 112821.

10 S. Koppala, R. Balan, I. Banerjee, K. Li, L. Xu, H. Liu, *et al.*, Room temperature synthesis of novel worm like tin oxide nanoparticles for photocatalytic degradation of organic pollutants, *Mater. Sci. Energy Technol.*, 2021, **4**, 113–118.

11 G. Elango and S. M. Roopan, Efficacy of SnO2 nanoparticles toward photocatalytic degradation of methylene blue dye, *J. Photochem. Photobiol., B*, 2016, **155**, 34–38.

12 S. P. Kim, M. Y. Choi and H. C. Choi, Photocatalytic activity of SnO2 nanoparticles in methylene blue degradation, *Mater. Res. Bull.*, 2016, **74**, 85–89.

13 A. Kar, S. Sain, S. Kundu, A. Bhattacharyya, S. Kumar Pradhan and A. Patra, Influence of size and shape on the photocatalytic properties of SnO2 nanocrystals, *ChemPhysChem*, 2015, **16**(5), 1017–1025.

14 Y. Sun, S. Zhang, B. Jin and S. Cheng, Efficient degradation of polyacrylamide using a 3-dimensional ultra-thin SnO2-Sb coated electrode, *J. Hazard. Mater.*, 2021, **416**, 125907.

15 A. Bhattacharjee and M. Ahmaruzzaman, Photocatalytic-degradation and reduction of organic compounds using SnO2 quantum dots (via a green route) under direct sunlight, *RSC Adv.*, 2015, **5**(81), 66122–66133.

16 R. Rahmayeni, Y. Oktavia, Y. Stiadi, S. Arief and Z. Zulhadjri, Spinel ferrite of MnFe2O4 synthesized in Piper betle Linn extract media and its application as photocatalysts and antibacterial, *J. Dispersion Sci. Technol.*, 2021, **42**(3), 465–474.

17 G. Preethi, A. S. Ninan, K. Kumar, R. Balan and H. Nagaswarupa, Molten salt synthesis of nanocrystalline ZnFe2O4 and its photocatalytic dye degradation studies, *Mater. Today: Proc.*, 2017, **4**(11), 11816–11819.

18 G. Xian, S. Kong, Q. Li, G. Zhang, N. Zhou, H. Du, *et al.*, Synthesis of Spinel Ferrite MFe2O4 (M= Co, Cu, Mn, and Zn) for Persulfate Activation to Remove Aqueous Organics: Effects of M-Site Metal and Synthetic Method, *Front. Chem.*, 2020, **8**, 177.

19 Y. Li, J. Shen, Y. Hu, S. Qiu, G. Min, Z. Song, *et al.*, General flame approach to chainlike MFe2O4 spinel (M= Cu, Ni, Co, Zn) nanoaggregates for reduction of nitroaromatic compounds, *Ind. Eng. Chem. Res.*, 2015, **54**(40), 9750–9757.

20 A. Manikandan, M. Durka and S. A. Antony, Hibiscus rosa-sinensis leaf extracted green methods, magneto-optical and catalytic properties of spinel CuFe 2 O 4 nano-and microstructures, *J. Inorg. Organomet. Polym. Mater.*, 2015, **25**(5), 1019–1031.

21 Y. Haihua, Y. Jianhui, H. Yueyang, L. Zhouguang, C. Xiang and T. Yougen, Photocatalytic activity evaluation of tetragonal CuFe {sub 2} O {sub 4} nanoparticles for the H {sub 2} evolution under visible light irradiation, *J. Alloys Compd.*, 2009, 476.

22 B. Surendra, M. Veerabhdraswamy, K. Anantharaju, H. Nagaswarupa and S. Prashantha, Green and chemical-engineered CuFe 2 O 4: characterization, cyclic voltammetry, photocatalytic and photoluminescent investigation for multifunctional applications, *J. Nanostruct. Chem.*, 2018, **8**(1), 45–59.

23 L. Wang, G. Hu, Z. Wang, B. Wang, Y. Song and H. Tang, Highly efficient and selective degradation of methylene blue from mixed aqueous solution by using monodisperse

CuFe 2 O 4 nanoparticles, *RSC Adv.*, 2015, **5**(90), 73327–73332.

24 M. Rashad, R. Mohamed, M. Ibrahim, L. Ismail and E. Abdel-Aal, Magnetic and catalytic properties of cubic copper ferrite nanopowders synthesized from secondary resources, *Adv. Powder Technol.*, 2012, **23**(3), 315–323.

25 Y. Guo, L. Zhang, X. Liu, B. Li, D. Tang, W. Liu, *et al.*, Synthesis of magnetic core–shell carbon dot@ MFe 2 O 4 (M= Mn, Zn and Cu) hybrid materials and their catalytic properties, *J. Mater. Chem. A*, 2016, **4**(11), 4044–4055.

26 H. Yang, J. Yan, Z. Lu, X. Cheng and Y. Tang, Photocatalytic activity evaluation of tetragonal CuFe2O4 nanoparticles for the H2 evolution under visible light irradiation, *J. Alloys Compd.*, 2009, **476**(1–2), 715–719.

27 X. Li, M. Zuo, J. Wu, L. Feng, Z. Wang and B. Liu, Wet chemistry synthesis of CuFe2O4/CdSe heterojunction for enhanced efficient photocatalytic H2 evolution under visible irradiation, *Int. J. Hydrogen Energy*, 2021, **46**(24), 13001–13010.

28 R. Noroozi, M. Gholami, M. Farzadkia and A. J. Jafari, Catalytic potential of CuFe 2 O 4/GO for activation of peroxymonosulfate in metronidazole degradation: study of mechanisms, *J. Environ. Health Sci. Eng.*, 2020, **18**(2), 947–960.

29 S. Rajabi, A. Nasiri and M. Hashemi, Enhanced activation of persulfate by CuCoFe2O4@MC/AC as a novel nanomagnetic heterogeneous catalyst with ultrasonic for metronidazole degradation, *Chemosphere*, 2022, **286**, 131872.

30 Y. Yao, F. Lu, Y. Zhu, F. Wei, X. Liu, C. Lian, *et al.*, Magnetic core–shell CuFe2O4@ C3N4 hybrids for visible light photocatalysis of Orange II, *J. Hazard. Mater.*, 2015, **297**, 224–233.

31 R. Li, M. Cai, Z. Xie, Q. Zhang, Y. Zeng, H. Liu, *et al.*, Construction of heterostructured CuFe2O4/g-C3N4 nanocomposite as an efficient visible light photocatalyst with peroxydisulfate for the organic oxidation, *Appl. Catal. B Environ.*, 2019, **244**, 974–982.

32 K. Cui, M. Sun, J. Zhang, J. Xu, Z. Zhai, T. Gong, *et al.*, Facile solid-state synthesis of tetragonal CuFe2O4 spinels with improved infrared radiation performance, *Ceram. Int.*, 2021, **48**(8), 10555–10561.

33 N. El Messaoudi, M. El Khomri, A. Dabagh, Z. G. Chegini, A. Dbik, S. Bentahar, *et al.*, Synthesis of a novel nanocomposite based on date stones/CuFe2O4 nanoparticles for eliminating cationic and anionic dyes from aqueous solution, *Int. J. Environ. Stud.*, 2021, 1–19.

34 Y. Zhang, A. Sun, M. Xiong, D. K. Macharia, J. Liu, Z. Chen, *et al.*, TiO2/BiOI pn junction-decorated carbon fibers as weavable photocatalyst with UV–vis photoresponsive for efficiently degrading various pollutants, *Chem. Eng. J.*, 2021, **415**, 129019.

35 T. Kondo, J.-j Hayafuji and H. Munekata, Investigation of Spin Voltaic Effect in a p–n Heterojunction, *Jpn. J. Appl. Phys.*, 2006, **45**(26), L663–L665, DOI: **10.1143/JJAP.45.L663**.

36 C.-l Hu, K.-j Jin, P. Han, H.-b Lu, L. Liao and G.-z Yang, The effect of phase separation on the temperature dependent magnetoresistance in perovskite oxide heterojunction, *Appl. Phys. Lett.*, 2008, **93**(16), 162106.

37 M. Golshan, B. Kakavandi, M. Ahmadi and M. Azizi, Photocatalytic activation of peroxymonosulfate by TiO2 anchored on cupper ferrite (TiO2@ CuFe2O4) into 2, 4-D degradation: process feasibility, mechanism and pathway, *J. Hazard. Mater.*, 2018, **359**, 325–337.

38 M. M. R. Khan, M. R. Uddin, H. Abdullah, K. M. R. Karim, A. Yousuf, C. K. Cheng, *et al.*, Preparation and characterization of CuFe2O4/TiO2 photocatalyst for the conversion of CO2 into methanol under visible light, *International Journal of Chemical, Molecular, Nuclear, Materials and Metallurgical Engineering*, 2016, **10**, 1165–1172.

39 Y. Y. Yi and Z. H. Qiang, Reduced Graphene Oxide Coupled Magnetic CuFe2O4-TiO2 Nanoparticles with Enhanced Photocatalytic Activity for Methylene Blue Degradation, *Chin. J. Struct. Chem.*, 2016, **35**(3), 472–480.

40 B. Janani, A. Syed, A. M. Thomas, S. Al-Rashed, A. M. Elgorban, L. L. Raju, *et al.*, A simple approach for the synthesis of bi-functional pn type ZnO@ CuFe2O4 heterojunction nanocomposite for photocatalytic and antimicrobial application, *Phys. E*, 2021, **130**, 114664.

41 E. A. Afshar and M. A. Taher, New fabrication of CuFe2O4/PAMAM nanocomposites by an efficient removal performance for organic dyes: Kinetic study, *Environ. Res.*, 2022, **204**, 112048.

42 W. Zhao, Y. Jin, C. Gao, W. Gu, Z. Jin, Y. Lei, *et al.*, A simple method for fabricating p–n junction photocatalyst CuFe2O4/Bi4Ti3O12 and its photocatalytic activity, *Mater. Chem. Phys.*, 2014, **143**(3), 952–962.

43 K. Ali, J. Iqbal, T. Jan, D. Wan, N. Ahmad, I. Ahamd, *et al.*, Structural, dielectric and magnetic properties of SnO2-CuFe2O4 nanocomposites, *J. Magn. Magn. Mater.*, 2017, **428**, 417–423.

44 A. Bhardwaj, A. Kumar, U. Sim, H.-N. Im and S.-J. Song, Synergistic enhancement in the sensing performance of a mixed-potential NH3 sensor using SnO2@CuFe2O4 sensing electrode, *Sens. Actuators, B*, 2020, **308**, 127748.

45 C. Karunakaran, S. SakthiRaadha, P. Gomathisankar and P. Vinayagamoorthy, Nanostructures and optical, electrical, magnetic, and photocatalytic properties of hydrothermally and sonochemically prepared CuFe 2 O 4/SnO 2, *RSC Adv.*, 2013, **3**(37), 16728–16738.

46 C. Xie, L. Xu, Y. Xia, R. Gang, Q. Ye and S. Koppala, Evaluation of visible photocatalytic performance of microwave hydrothermal synthesis of MnO2/TiO2 core-shell structures and gaseous mercury removal, *Microporous Mesoporous Mater.*, 2022, **334**, 111788.

47 R. Gang, Y. Xia, L. Xu, L. Zhang, S. Ju, Z. Wang, *et al.*, Size controlled Ag decorated TiO2 plasmonic photocatalysts for tetracycline degradation under visible light, *Surface. Interfac.*, 2022, 102018.

48 K. G. Godinho, A. Walsh and G. W. Watson, Energetic and Electronic Structure Analysis of Intrinsic Defects in SnO2, *J. Phys. Chem. C*, 2009, **113**(1), 439–448.

49 X. Zhao, W. Wu, G. Jing and Z. Zhou, Activation of sulfite autoxidation with CuFe2O4 prepared by MOF-templated

method for abatement of organic contaminants, *Environ. Pollut.*, 2020, **260**, 114038.

50 J. Tauc, R. Grigorovici and A. Vancu, Optical Properties and Electronic Structure of Amorphous Germanium, *Phys. Status Solidi B*, 1966, **15**(2), 627–637.

51 S. Koppala, R. Balan, I. Banerjee, K. Li, L. Xu, H. Liu, *et al.*, Room temperature synthesis of novel worm like tin oxide nanoparticles for photocatalytic degradation of organic pollutants, *Mater. Sci. Energy Technol.*, 2021, **4**, 113–118.

52 S. David, M. A. Mahadik, H. S. Chung, J. H. Ryu and J. S. Jang, Facile Hydrothermally Synthesized a Novel CdS Nanoflower/Rutile-TiO2 Nanorod Heterojunction Photoanode Used for Photoelectrocatalytic Hydrogen Generation, *ACS Sustainable Chem. Eng.*, 2017, **5**(9), 7537–7548.

53 S. Le, W. Yang, G. Chen, A. Yan and X. Wang, Extensive solar light harvesting by integrating UPCL C-dots with Sn2Ta2O7/SnO2: Highly efficient photocatalytic degradation toward amoxicillin, *Environ. Pollut.*, 2020, **263**, 114550.